

SiDGen: Structure-informed Diffusion for Generative Modeling of Ligands for Proteins

Samyak Sanghvi¹ Nishant Ranjan¹ Tarak Karmakar²

Abstract

Structure-based drug design (SBDD) faces a fundamental **scaling fidelity dilemma**: rich pocket-aware conditioning captures interaction geometry but can be costly, often scales quadratically ($O(L^2)$) or worse with protein length (L), while efficient sequence-only conditioning can miss key interaction structure. We propose **SiDGen**, a structure-informed discrete diffusion framework that resolves this trade-off through a **Topological Information Bottleneck (TIB)**. SiDGen leverages a learned, soft assignment mechanism to compress residue-level protein representations into a compact bottleneck enabling downstream pairwise computations on the coarse grid ($O(L^2/s^2)$). This design reduces memory and computational cost without compromising generative accuracy. Our approach achieves state-of-the-art performance on CrossDocked2020 and DUD-E benchmarks while significantly reducing pairwise-tensor memory. SiDGen bridges the gap between sequence-based efficiency and pocket-aware conditioning, offering a scalable path for high-throughput structure-based discovery. ¹

1. Introduction

The computational search for novel therapeutics involves navigating a chemical space of approximately 10^{60} drug-like molecules. Within this space, structure-based drug design (SBDD) aims to generate ligands that exhibit high binding affinity and specificity for a target protein pocket. Recent advancements in deep generative modeling, particularly denoising diffusion models (Hoogeboom et al., 2022; Vignac

¹Department of Computer Science, Indian Institute of Technology, Delhi, India ²Department of Chemistry, Indian Institute of Technology, Delhi, India. Correspondence to: Samyak Sanghvi <samyakssanghvi@gmail.com>, Tarak Karmakar <tkarmakar@chemistry.iitd.ac.in>.

Preprint. February 2, 2026.

¹The code with instructions can be found at <https://github.com/SamyakSS83/SiDGEN/>

et al., 2023), have shown significant promise in generating chemically diverse and geometrically accurate molecules. However, when applied to protein-conditioned generation, these models face a critical **scaling-fidelity dilemma**.

The Scaling-Fidelity Dilemma. High-fidelity structural generative models typically operate on atomic point clouds or fine-grained graph representations of protein pockets. (Guan et al., 2023a; Peng et al., 2025) To capture the intricate complementarity between a ligand and its receptor, these models employ $E(3)$ -equivariant neural networks or dense transformer architectures that compute all-to-all interactions. Although expressive, the memory and computational costs of such operations scale quadratically ($O(L^2)$) or even cubically with the number of protein residues L . This ‘computational wall’ limits the ability of practitioners to process large proteins or handle multi-target discovery campaigns where throughput is essential.

In contrast, sequence-centric models utilize pre-trained protein language models (pLMs) such as ESM-2 (Lin et al., 2022) to provide efficient, linear-time conditioning ($O(L)$). Although these pLMs capture rich evolutionary and implicit structural semantics, they are often used as ‘black-box’ sequence embeddings that fail to explicitly model the 3D topological information of a specific binding pocket. As a result, such approaches often generate molecules that are chemically valid yet ‘target-agnostic’, lacking the geometric specificity necessary for high affinity and selective binding.

SiDGen: Resolving the Dilemma via Topological Information Bottlenecks. In this work, we propose **SiDGen** (Structure-informed Diffusion Generator), a framework that bridges the gap between sequence efficiency and structural awareness. Our approach is based on the observation that while individual residue interactions are fine-grained, the *complementarity* of a binding pocket is often governed by persistent topological clusters, arrangements of secondary structure elements, and conserved motifs that define the geometry of the binding pocket. (Guharoy & Chakrabarti, 2010)

We formalize this observation through the concept of a **Topological Information Bottleneck (TIB)**. SiDGen learns to pool dense residue-level features into a compact, coarse-

grained bottleneck representation $z \in \mathbb{R}^{K \times d}$, where $K \ll L$. Using a DiffPool-inspired soft assignment mechanism (Ying et al., 2018), the model dynamically identifies a subset of residues that form critical interaction units. This aggregation reduces the complexity of subsequent generative operations from $O(L^2)$ to $O(K^2)$, enabling scalable processing of large proteins (e.g., $L = 2000$) on consumer-grade hardware while preserving the essential structural context.

Chemformer-style Discrete Diffusion. To ensure that the generated molecules are both chemically robust and target-responsive, SiDGen operates in the discrete space of SMILES strings using a Chemformer-style tokenizer and transformer denoiser architecture (Irwin et al., 2021). Masked diffusion in the SMILES space allows the model to leverage strong chemical priors while being precisely conditioned on the topological bottleneck. We augment this process with training-time stability components, including an in-loop validity penalty and a curriculum-based noise schedule.

Summary of Contributions.

- We introduce the **Topological Information Bottleneck** as a principled framework for efficient structural conditioning in SBDD.
- We propose **SiDGen**, integrating a hierarchical soft-assignment structural encoder (DiffPool-inspired) with a Chemformer-style discrete diffusion backbone, achieving $O(K^2)$ scaling.
- We provide an exhaustive empirical evaluation on **MOSES**, **CrossDocked2020**, and **DUD-E** benchmarks, including a comparison with recent state-of-the-art models such as **RxnFlow** (Seo et al., 2025), **CIDD** (Gao et al., 2025), and **MolJO** (Qiu et al., 2025).
- We demonstrate a superior **compute-quality Pareto front**, showing that SiDGen maintains high enrichment factors while using $\sim 94\%$ less end-to-end VRAM than full structural conditioning baselines.

The resulting SiDGen framework achieves a Vina Docking score of -9.81 kcal/mol and an enrichment factor EF@1% of 10.26 on the DUD-E benchmark. These results demonstrate that high-fidelity pocket-aware ligand generation can be achieved without the quadratic scaling overhead associated with fine-grained structural modeling.

2. Background

2.1. Discrete Diffusion in Chemical Space

Diffusion models for discrete data, such as SMILES strings or molecular graphs, differ from their continuous counterparts in their corruption process. Given a ligand $x_0 \in \mathcal{V}^M$ from a vocabulary \mathcal{V} of size V , the forward process $q(x_t | x_{t-1})$ is defined by a transition matrix $\mathbf{Q}_t \in [0, 1]^{V \times V}$. The probability of being in state j at time t given state i at time 0 is:

$$q(x_t = j | x_0 = i) = [x_0 \bar{\mathbf{Q}}_t]_j \quad (1)$$

where $\bar{\mathbf{Q}}_t = \prod_{s=1}^t \mathbf{Q}_s$. In practice, \mathbf{Q}_t is often parametrized as a mixture of identity and uniform noise distribution, resulting in a closed form expression for $q(x_t | x_0)$.

In **SiDGen**, we employ a masking transition in which a token is replaced by a special [MASK] token with probability $\sigma(t)$. This transition preserves the structural identity of unmasked tokens, allowing the model to focus on denoising specific chemical motifs within the protein’s structural context.

3. Related Work

3.1. Generative Models for SBDD

The field of structure-based *de novo* design has transitioned from search-based methods to deep generative modeling. The early benchmarks were dominated by autoregressive models and VAEs (Gómez-Bombarelli et al., 2016). More recently, diffusion models have set new benchmarks for 3D pose generation. **TargetDiff** (Guan et al., 2023a) and **Pocket2Mol** (Peng et al., 2025) utilize equivariant GNNs to model protein-ligand interactions in continuous space. Although effective, these models require full structural awareness, leading to quadratic scaling issues.

Recently, a new wave of models has emerged to improve geometric feasibility and practical drug-likeness. Qu et al. (2024) propose **MolCRAFT** – an SBDD generative model that operates in a continuous parameter space with a noise-reduced sampling strategy to improve pose stability and binding affinity. **MolJO** (Qiu et al., 2025) studies the coupling between discrete (2D topology) and continuous (3D geometry) modalities and proposes an improved noise scheduling strategy to improve interaction modeling and pose quality. In parallel, **RxnFlow** (Seo et al., 2025) incorporates reaction-aware constraints, while **CIDD** (Gao et al., 2025) leverages collaboration between physics-based structure signals and large language models. SiDGen is complementary: rather than redesigning the 3D generator, we target the *scaling bottleneck* by compressing the protein conditioning signal into a learnable topological bottleneck.

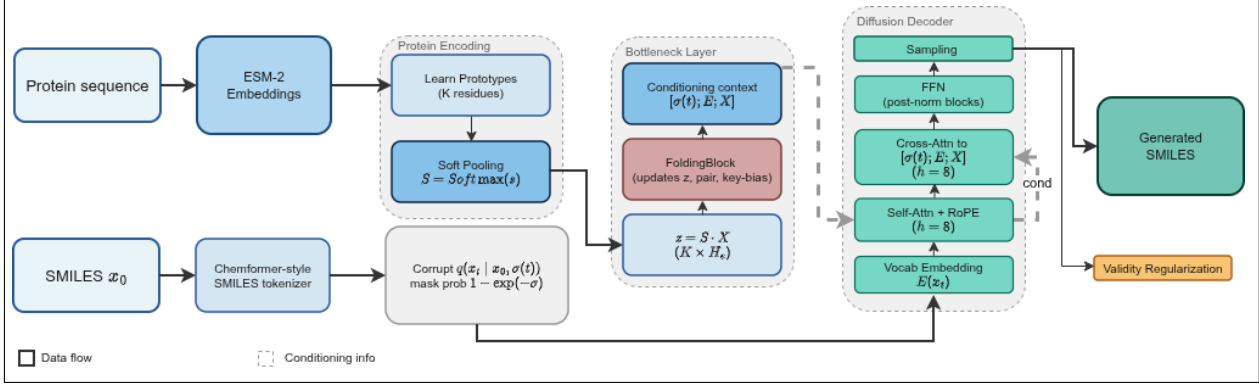


Figure 1. Overview of the SiDGen architecture. A target protein is processed through a hierarchical structural encoder to produce a Topological Information Bottleneck z , which conditions a Chemformer-style discrete diffusion process in SMILES space.

3.2. Discrete Denoising and Language Models

The success of transformers in chemical space (Irwin et al., 2021; Ross et al., 2021) has led to several SMILES-based diffusion models. **LDMol** (Chang & Ye, 2025) demonstrates that operating in string space allows models to capture long-range chemical dependencies that are often missed by graph-based methods. However, conditioning these models on 3D structures without linear-time approximations remains a challenge. Our work integrates the learned pooling of the protein representation with an efficient SMILES-diffusion backbone.

3.3. Efficiencies in Protein Modeling

Efforts to scale protein modeling include MSA-subsampling and token-dropping in ESM-like models. However, these are often fixed heuristics. Learnable pooling approaches have been successful in fold classification, but have seen limited use as conditioning bottlenecks for generative tasks. Our **Topological Information Bottleneck (TIB)** is inspired by these hierarchical representations but optimized specifically for ligand complementarity.

4. Methodology

4.1. Hierarchical Structural Diffusion (HSD)

We formulate protein-conditioned ligand generation as a conditional diffusion process $p(x | \mathcal{P})$, where x is a ligand SMILES string, and $\mathcal{P} \in \mathbb{R}^{K \times d_p}$ is the target protein representation (ESM-2 residue embeddings). To resolve the scaling-fidelity dilemma, we decompose the conditioning signal into a (**TIB**). Specifically, we learn a compact representation $z = \mathcal{F}_{\text{pool}}(\mathcal{P})$, where $z \in \mathbb{R}^{K \times d}$ and $K \ll L$. The density of the conditioning information is controlled by the stride parameter s , such that $K \approx \lceil L/s \rceil$.

In our implementation, the bottleneck is computed deter-

ministically, and we model

$$p(x | \mathcal{P}) = p(x | z(\mathcal{P})). \quad (2)$$

That is, $p(z | \mathcal{P})$ is implemented as a deterministic pooling module over residue embeddings (Sec. 4.2). The conditional distribution $p(x | z)$ is defined by a transformer-based denoiser operating in the SMILES space within the discrete diffusion framework.

4.2. Topological Information Bottleneck via Soft Assignment Pooling

The core of SiDGen’s efficiency lies in the learnable pooling mechanism. Unlike fixed downsampling, which can indiscriminately discard important residues in the binding pocket, our prototype-based soft assignment pooling (DiffPool-inspired) learns a soft assignment matrix $S \in \mathbb{R}^{L \times K}$ that preserves the topological integrity (neighbourhood and connectivity) of the protein active site.

Why this pooling is adaptive and information-preserving. The assignment weights $S_{b,i,k}$ are calculated from learned projections of residue tokens and prototypes, so the pooling is *input-dependent*: residues that are most informative for the target (e.g., pocket residues) can be assigned with higher mass to a small subset of bottleneck tokens. Moreover, the pooled token $z_{b,k} = \sum_i S_{b,i,k} \mathbf{X}_{b,i}$ is a convex combination of residue embeddings; this preserves information in the sense that each bottleneck token remains in the span of the original residue features while enabling end-to-end differentiability through S .

Encoder Architecture. Given residue embeddings $\mathbf{X} \in \mathbb{R}^{B \times L \times d}$, we first form $K = \lceil L/s \rceil$ pooled prototypes. We compute soft assignments using learned projections and

scaled dot-product similarity:

$$\ell_{b,i,k} = \frac{\langle \phi_{\text{tok}}(\mathbf{X}_{b,i}), \phi_{\text{proto}}(\mathbf{P}_{b,k}) \rangle}{\sqrt{d}}, \quad (3)$$

$$\mathbf{S}_{b,i,:} = \text{softmax}(\ell_{b,i,:}). \quad (4)$$

For each batch element b , residue i , and prototype k , we compute a similarity score $\ell_{b,i,k}$ as the dot product between the projected residue and prototype embeddings, scaled by \sqrt{d} . A softmax over k gives the assignment weights, $\mathbf{S}_{b,i,:}$. We mask padded residues and invalid prototypes before the softmax.

The bottleneck tokens are pooled as weighted aggregation of the residue embeddings,

$$\mathbf{z}_{b,k} = \sum_{i=1}^L \mathbf{S}_{b,i,k} \mathbf{X}_{b,i} \in \mathbb{R}^d, \quad \Rightarrow \quad \mathbf{z} \in \mathbb{R}^{B \times K \times d}. \quad (5)$$

This bottleneck is compact enough to support coarse-grid pairwise computations and efficient cross-attention conditioning in the diffusion model.

4.3. Chemformer Interface and Discrete Diffusion

SiDGen utilizes a transformer-based denoiser with a Chemformer-style tokenizer/architecture (Irwin et al., 2021) as the denoising network f_θ . The input to the decoder is a masked SMILES sequence $x_t \in \{s_1, \dots, s_M\}$.

Ligand tokenization and embeddings. We represent each ligand as a sequence of token IDs produced by a Chemformer-style SMILES tokenizer, including special tokens such as [PAD] and [MASK]. Let $x_t \in \{1, \dots, V\}^{B \times L_{\text{lig}}}$ denote the (possibly corrupted) token IDs at diffusion time t . The denoiser maps token IDs to continuous vectors *via* a learned embedding table $\text{Embed} : \{1, \dots, V\} \rightarrow \mathbb{R}^H$, producing initial ligand hidden states

$$\mathbf{H}^{(0)} = \text{Embed}(x_t) \in \mathbb{R}^{B \times L_{\text{lig}} \times H}. \quad (6)$$

These embeddings are then processed by a transformer decoder stack with rotary position embeddings (RoPE) in the ligand self-attention layers.

Topological Conditioning. The pooled protein representation is injected into every layer of the transformer decoder *via* cross-attention over the conditioning tokens $\mathbf{E} \in \mathbb{R}^{B \times K \times H}$. For a ligand query vector $q_i \in \mathbb{R}^H$, the attention update is:

$$\text{CrossAttn}(q_i, \mathbf{E}) = \text{softmax} \left(\frac{q_i \mathbf{W}_Q (\mathbf{E} \mathbf{W}_K)^\top}{\sqrt{H}} \right) (\mathbf{E} \mathbf{W}_V). \quad (7)$$

By querying the compressed structural features \mathbf{E} , the ligand generator incorporates protein context without attending over all L_{prot} residues.

4.4. Decoder Architecture

The denoiser is a multi-layer Transformer decoder that updates ligand hidden states via (i) ligand self-attention (with RoPE) and (ii) cross-attention into a protein-derived conditioning context. In this section, we use $\mathbf{X}_\ell \in \mathbb{R}^{B \times L_{\text{lig}} \times H}$ for the ligand hidden states at decoder layer ℓ ; protein residue embeddings are denoted separately as $\mathbf{X}^{\text{prot}} \in \mathbb{R}^{B \times L_{\text{prot}} \times d}$.

Inputs:

- (i) $t \in \mathbb{R}^B$: scalar timesteps for each batch element $b = 1, \dots, B$.
- (ii) $x_t \in \{1, \dots, V\}^{B \times L_{\text{lig}}}$: ligand token IDs after corruption at diffusion time t .
- (iii) $\mathbf{X}_0 = \text{Embed}(x_t) \in \mathbb{R}^{B \times L_{\text{lig}} \times H}$: embedded ligand tokens (decoder input states).
- (iv) $\mathbf{E} \in \mathbb{R}^{B \times K \times H}$: bottleneck conditioning tokens of length K (typically $K = \lceil L_{\text{prot}}/s \rceil$), obtained by pooling protein features and projecting to hidden size H .

Timestep Embeddings: Sinusoidal encodings are projected through a two-layer MLP with SiLU (Elfwing et al., 2017) activations to form the timestep token:

$$\sigma(t) = \text{SiLU}(W_2 \text{SiLU}(W_1 \text{PE}(t))), \quad \sigma(t) \in \mathbb{R}^H. \quad (8)$$

Conditioning context: The diffusion timestep is embedded as a single token and prepended to the conditioning tokens to form the cross-attention key/value sequence

$$\mathbf{C}_{\text{cond}} = [\sigma(t); \mathbf{E}; \mathbf{X}^{\text{prot}}]. \quad (9)$$

Rotary Position Embeddings (RoPE) (Su et al., 2021):

$$\text{RoPE}(x_m, m) = R(m)x_m, \quad (10)$$

$$R(m) = \begin{pmatrix} \cos(m\theta) & -\sin(m\theta) \\ \sin(m\theta) & \cos(m\theta) \end{pmatrix}, \quad (11)$$

$$\theta = 10000^{-2i/d}, \quad (12)$$

where x_m is the m -th token embedding, m is the position index, and $d = H/h$ is the per-head dimension.

Multi-Head Attention Mechanism Each decoder layer ℓ applies the following operations sequentially:

(i) Self-Attention on Ligand Tokens: The ligand sequence attends to itself to capture intra-molecular dependencies:

$$Q_{\text{lig}} = \mathbf{X}_{\ell-1} W_Q^{\text{self}}, \quad (13)$$

$$K_{\text{lig}} = \mathbf{X}_{\ell-1} W_K^{\text{self}}, \quad V_{\text{lig}} = \mathbf{X}_{\ell-1} W_V^{\text{self}}, \quad (14)$$

$$\mathbf{A}_{\text{self}} = \text{Softmax} \left(\frac{Q_{\text{lig}} K_{\text{lig}}^T}{\sqrt{d}} \right) V_{\text{lig}}, \quad (15)$$

$$\mathbf{X}'_\ell = \text{LayerNorm}(\mathbf{X}_{\ell-1} + \mathbf{A}_{\text{self}}). \quad (16)$$

Here, the ligand tokens attend to each other to capture intra-SMILES dependencies; timestep information enters through cross-attention to \mathbf{C}_{cond} .

(ii) Cross-Attention with Conditioning Context: The ligand tokens query the conditioning context to incorporate target information:

$$Q_{\text{lig}} = \mathbf{X}'_{\ell} W_Q^{\text{cross}}, \quad (17)$$

$$K_{\text{cond}} = \mathbf{C}_{\text{cond}} W_K^{\text{cross}}, \quad V_{\text{cond}} = \mathbf{C}_{\text{cond}} W_V^{\text{cross}}, \quad (18)$$

$$\mathbf{A}_{\text{cross}} = \text{Softmax} \left(\frac{Q_{\text{lig}} K_{\text{cond}}^T}{\sqrt{d}} \right) V_{\text{cond}}, \quad (19)$$

$$\mathbf{X}''_{\ell} = \text{LayerNorm}(\mathbf{X}'_{\ell} + \mathbf{A}_{\text{cross}}). \quad (20)$$

This operation allows each ligand token to attend to all conditioning tokens, aggregating relevant target information. In our implementation, \mathbf{C}_{cond} is formed from the timestep token and bottleneck tokens (and the full residue sequence embeddings from ESM-2).

(iii) Feed-Forward Network: Position-wise MLP with residual connection:

$$\text{FFN}(x) = W_2 \text{ReLU}(W_1 x + b_1) + b_2, \quad (21)$$

$$\mathbf{X}_{\ell} = \text{LayerNorm}(\mathbf{X}''_{\ell} + \text{FFN}(\mathbf{X}''_{\ell})). \quad (22)$$

The final layer output is projected to vocabulary logits for token prediction.

4.5. Coarse Folding of Structural Features on the Bottleneck Grid

Coarsening with stride s . Before learned pooling, we define a simple coarsening operator that subsamples residues at stride s to form a coarse grid of size $K = \lceil L/s \rceil$. Let $\mathcal{I}_s = \{0, s, 2s, \dots\}$ be the strided index set. For single and pair features,

$$\mathbf{s}^{(s)} = \mathbf{s}[\mathcal{I}_s] \in \mathbb{R}^{B \times K \times C_{\text{single}}}, \quad (23)$$

$$\mathbf{p}^{(s)} = \mathbf{p}[\mathcal{I}_s, \mathcal{I}_s] \in \mathbb{R}^{B \times K \times K \times C_{\text{pair}}}. \quad (24)$$

This fixed coarsening reduces memory from $O(L^2)$ to $O(K^2)$, and serves as the baseline we compare against our learned bottleneck.

To mitigate the quadratic scaling of structural features, we employ a learnable soft assignment mechanism inspired by DiffPool (Ying et al., 2018). Given protein sequence embeddings $\mathbf{X} \in \mathbb{R}^{B \times L \times d}$, we learn an assignment matrix that pools residue embeddings to a coarser resolution.

Soft Assignment Matrix We compute $\mathbf{S} \in \mathbb{R}^{B \times L \times K}$ using strided prototypes and learned projections (Sec. 4.2). This yields a lightweight soft clustering while keeping computation efficient.

Coarse Pair Construction We pool residue embeddings into bottleneck tokens $\mathbf{z} \in \mathbb{R}^{B \times K \times d}$, and then construct coarse pair features directly on the bottleneck grid:

$$\mathbf{p}_c = \text{OuterLinearPair}(\mathbf{z}) \in \mathbb{R}^{B \times K \times K \times C_{\text{pair}}}. \quad (25)$$

This avoids forming any full-resolution $L \times L$ pair tensor and yields the claimed $O(K^2)$ pairwise footprint.

Folding Operations On the coarse pair features $\mathbf{p}_c \in \mathbb{R}^{B \times K \times K \times C_{\text{pair}}}$, we apply triangle attention and triangle multiplication inspired by AlphaFold (Jumper et al., 2021):

Triangle Attention:

$$\text{TriAttn}_{\text{start}}(\mathbf{p}_c) : \quad \mathbf{p}_c[b, i, j] \leftarrow \text{Attention}_k(\mathbf{p}_c[b, i, k]), \quad (26)$$

$$\text{TriAttn}_{\text{end}}(\mathbf{p}_c) : \quad \mathbf{p}_c[b, i, j] \leftarrow \text{Attention}_k(\mathbf{p}_c[b, k, j]). \quad (27)$$

Triangle Multiplication:

$$\text{TriMult}_{\text{out}}(\mathbf{p}_c) : \quad \mathbf{p}_c[b, i, j] \leftarrow \sum_k \mathbf{p}_c[b, i, k] \odot \mathbf{p}_c[b, j, k], \quad (28)$$

$$\text{TriMult}_{\text{in}}(\mathbf{p}_c) : \quad \mathbf{p}_c[b, i, j] \leftarrow \sum_k \mathbf{p}_c[b, k, i] \odot \mathbf{p}_c[b, k, j]. \quad (29)$$

These operations process the coarse structure, updating pairwise relationships among the K bottleneck tokens. Triangle attention is quadratic in K , while triangle multiplication additionally contracts over K ($O(K^3)$).

Decoder Conditioning The decoder consumes the processed bottleneck tokens as conditioning. We derive a coarse cross-attention key-bias per head from aggregated coarse pair features.

Complexity Analysis The bottleneck-based mechanism reduces memory and compute while enabling learned feature aggregation:

- **Memory:** Pair features scale as $O(L^2) \rightarrow O(K^2)$ where $K = \lceil L/s \rceil$. For $s = 4$, this yields $\sim 16 \times$ reduction.
- **Compute:** Triangle attention/multiplication operations scale as $O(K^2 \cdot K) = O(K^3)$ vs. $O(L^3)$, providing $\sim s^3 = 64 \times$ speedup for $s = 4$.
- **Assignment overhead:** Computing \mathbf{S} requires $O(L \cdot K)$ operations, which is negligible compared to the $O(L^2)$ savings.

- **Gradient flow:** Unlike fixed downsampling, soft assignments enable end-to-end learning, allowing the model to adapt pooling to task-specific structural patterns.

4.6. Training Enhancements

Substitution Parameterization: masked diffusion loss with substitution scaling:

$$\mathcal{L}_{\text{MDLM}} = - \sum_{i,t} \log p_{\theta}(x_0^{(i)} | x_t^{(i)}, c) \cdot \frac{d\sigma/dt}{\exp(\sigma) - 1}. \quad (30)$$

Masking corruption: we sample $t \sim \text{Uniform}(0, 1)$, compute a noise level $\sigma(t)$, and independently replace each token with [MASK] with probability $1 - \exp(-\sigma(t))$.

Curriculum Learning To gradually increase the difficulty of the denoising task, we scale the timestep used for loss computation:

$$t_{\text{curriculum}} = \min(\max(\epsilon, \alpha_{\text{epoch}} t), 1), \quad (31)$$

$$\alpha_{\text{epoch}} = \min\left(1, \frac{\text{epoch} + 1}{T_{\text{curriculum}}}\right), \quad (32)$$

where $t \in [0, 1]$ is the diffusion timestep, $\epsilon > 0$ is a small lower bound, epoch is the current training epoch, and $T_{\text{curriculum}}$ is the total number of curriculum epochs.

In-loop Validity Penalty. We define a sample-based validity regularizer that directly targets the model’s empirical valid-generation rate. Formally the desideratum is

$$\mathcal{J}_{\text{valid}} = \mathbb{E}_{x \sim p_{\theta}} [\mathbf{1}_{x \text{ valid}}] \quad (33)$$

the expected fraction of valid SMILES under the model distribution. In practice, we approximate this expectation by Monte-Carlo: every N optimizer steps we decode S samples from the current model and compute the empirical validity

$$\hat{\mathcal{J}}_{\text{valid}} = \frac{1}{S} \sum_{i=1}^S \mathbf{1}_{x_i \text{ valid}}, \quad (34)$$

and optimize it using a score-function (REINFORCE) estimator. Because decoding and the validity indicator are non-differentiable, we do not backpropagate through the sampling/validation pipeline; instead, we attach gradients through the log-probability of the sampled sequence:

$$\nabla_{\theta} \mathbb{E}_{x \sim p_{\theta}} [\mathbf{1}_{x \text{ valid}}] = \mathbb{E}_{x \sim p_{\theta}} [\mathbf{1}_{x \text{ valid}} \nabla_{\theta} \log p_{\theta}(x)]. \quad (35)$$

Concretely, every N optimizer steps we sample S sequences, compute validity flags, and add the REINFORCE loss

$$\mathcal{L}_{\text{total}} = \mathcal{L}_{\text{MDLM}} - \lambda_{\text{valid}} \frac{1}{S} \sum_{i=1}^S (\mathbf{1}_{x_i \text{ valid}} - b) \log p_{\theta}(x_i), \quad (36)$$

where b is a moving baseline (implemented as the batch mean validity) to reduce gradient variance.

5. Experiments

5.1. Evaluation Framework and Datasets

We evaluate SiDGen across four complementary benchmarks to assess molecular quality, structural fidelity, and virtual screening performance.

- **MOSES** (Polykovskiy et al., 2020): Used for assessing unconditional molecular generation quality, including chemical validity, uniqueness, and novelty.
- **CrossDocked2020** (Francoeur et al., 2020): A large-scale protein-ligand dataset used to evaluate 3D binding affinity and pose reasonability.
- **DUD-E** (Mysinger et al., 2012): Evaluates high-throughput virtual screening capabilities using enrichment factors (EF@1%), FCD (Preuer et al., 2018) and BEDROC (Zhao et al., 2009) scores.

5.2. Molecular Quality on MOSES

Table 1 summarizes SiDGen’s performance on the MOSES benchmark. Our Chemformer-style transformer denoiser achieves 100% validity and competitive novelty (100%), significantly outperforming previous VAE and GAN-based baselines. The high uniqueness (88.75%) confirms that SiDGen does not simply memorize the training set but explores the latent chemical space efficiently.

Table 1. Molecular generation quality on the MOSES benchmark.

Method	Validity	Uniqueness	Novelty	IntDiv \uparrow
CharRNN	97.5%	99.9%	84.2%	0.856
VAE	97.7%	99.8%	69.5%	0.855
JTN-VAE	100%	99.9%	91.4%	0.855
SiDGen	100%	88.75%	100%	0.903

5.3. Structure-Based Benchmarks: CrossDocked2020

We evaluate SiDGen’s ability to generate target-specific ligands on the CrossDocked2020 test set. We compare SiDGen against both classical 3D generators and recent 2024-2025 SOTA models.

Table 2. Performance comparison on the CrossDocked2020 test set.

Model	Paradigm	Vina Dock ↓	QED ↑	SA ↑	Diversity ↑	Time(s) ↓
Pocket2Mol	3D Autoregressive	-7.25	0.56	0.76	0.86	2184
TargetDiff	3D Diffusion	-7.46	0.48	0.58	0.72	3156
DecompDiff	3D Decomposition	-8.39	0.45	0.61	0.87	5367
MolCRAFT	Fragment-based	-9.25	0.46	0.58	0.82	139
ProtoBindDiff	Diffusion Based	-9.03	0.55	0.33	0.88	143
RxnFlow	Reaction-aware	-8.85	0.67	0.35	0.81	4
CIDD	LLM-Guided 3D	-9.02	0.53	0.69	0.87	149
MolJO	Fragment Based Optimizer	-9.05	0.56	0.78	0.66	18
SiDGen (Ours)	HSD + TIB	-9.81	0.58	0.49	0.90	63

As shown in Table 2, SiDGen achieves a superior Vina Dock score of -9.81 kcal/mol, outperforming even recent physics-aware 3D generators. Crucially, SiDGen maintains significantly higher diversity (0.89), suggesting that the Topological Information Bottleneck allows for broader exploration of valid binding modes compared to rigid 3D coordinate-based sampling.

5.4. Virtual Screening Performance on DUD-E

To evaluate practical utility in drug discovery pipelines, we conduct a virtual screening study on the DUD-E dataset. We measure the model’s ability to rank active compounds above decoys.

Table 3. DUD-E Virtual Screening metrics. EF@1% measures early enrichment, while BEDROC assesses ranking quality.

Method	ROC-AUC	EF@1%	BEDROC
AutoDock Vina	0.697	8.82	0.15
Gnina	0.680	7.93	0.18
Glide SP	0.830	9.5	0.29
SiDGen	0.819	10.26	0.28

The competitive enrichment factor (EF@1% = 10.26) demonstrates that SiDGen’s structural conditioning is sufficient to distinguish subtle differences in binding complementarity, even without explicit 3D coordinate generation at inference time.

5.5. Training Components

Table 4 ablates curriculum learning and validity regularization on CrossDocked2020 benchmark.

Both components contribute synergistically: curriculum learning and validity regularization eliminate invalid outputs. Combined, they achieve perfect validity while getting better quality results than baseline.

Table 4. Ablation of training enhancements on CrossDocked2020

Folding	Curriculum	Val Penalty	Vina Dock	QED
✗	✗	✗	-9.03	0.55
✓	✗	✗	-9.26	0.53
✓	✓	✗	-9.66	0.54
✓	✗	✓	-9.57	0.56
✓	✓	✓	-9.74	0.58

5.6. Resolving the Scaling-Fidelity Dilemma

Pareto Analysis: Computation vs. Quality. We systematically vary the pooling stride s from 1 (dense) to 16 (ultra-coarse) to investigate the compute-quality trade-off. As shown in Figure 2, increasing the stride significantly reduces VRAM usage while maintaining robust binding scores. We additionally compare the learned soft-assignment bottleneck to a coarse strided pooling baseline (index-select downsampling in the folding block); learned pooling consistently yields better binding and fidelity at the same stride. We report this comparison in Appendix B (Table 6).

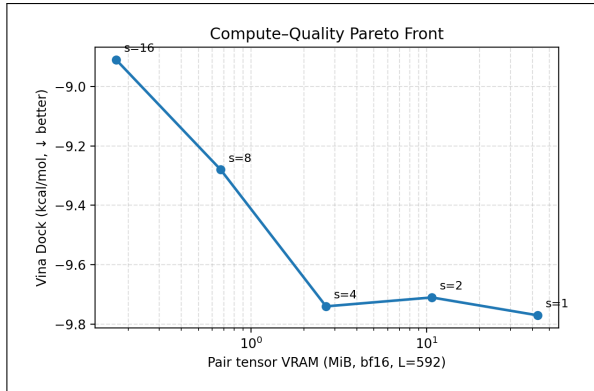


Figure 2. The Compute-Quality Pareto Front.

Pocket Fidelity Analysis. To quantify information loss induced by the bottleneck, we compute a *pocket-fidelity recovery* score on residues proximal to the bound ligand. For each

protein–ligand complex, let $\mathcal{I}_{\text{pocket}}$ be the set of residues with minimum heavy-atom distance $\leq 5 \text{ \AA}$ to any ligand heavy atom. We partition $\mathcal{I}_{\text{pocket}}$ into (i) hydrophobic-contact residues (hydrophobic sidechains within 5 \AA) and (ii) hydrogen-bond-capable residues (donor/acceptor sidechains within 5 \AA). For a given pooling stride s , we compute the bottleneck tokens \mathbf{z} and reconstruct residue-level embeddings as $\widehat{\mathbf{X}} = \mathbf{S}\mathbf{z}$.

We define the recovery score for a residue subset \mathcal{I} as the mean cosine similarity between original and reconstructed embeddings:

$$\text{Rec}(\mathcal{I}) = 100 \cdot \frac{1}{|\mathcal{I}|} \sum_{i \in \mathcal{I}} \frac{\langle \mathbf{X}_i, \widehat{\mathbf{X}}_i \rangle}{\|\mathbf{X}_i\| \|\widehat{\mathbf{X}}_i\|}. \quad (37)$$

This yields an interpretable percentage of how well pocket-local information is preserved by the bottleneck; learnable pooling attains 89.2% recovery at $s = 4$, whereas fixed-stride downsampling attains 61.1%.

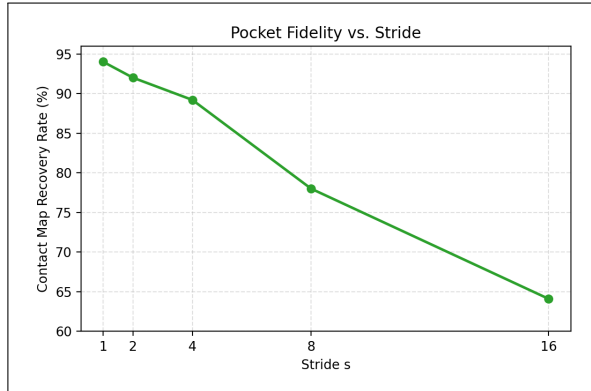


Figure 3. Pocket Fidelity Quantification: Percent recovery of hydrophobic and hydrogen-bond interactions within 5 \AA of the ligand.

6. Discussion

6.1. Innovation: The Topological Perspective

One common critique of string-based generative models for SBDD is their perceived lack of geometric awareness. However, we argue that the **Topological Information Bottleneck** (TIB) represents a shift from “physical modeling” to “topological abstraction.” While 3D coordinate generators attempt to satisfy physical constraints (e.g., steric clashing) through explicit force fields or $E(3)$ -equivariant updates, SiDGen learns to satisfy these constraints through latent topological descriptors.

The success of the TIB suggests that the chemical space of binding pockets is lower-dimensional than the raw coordinate space. By compressing L residues into K topological clusters, SiDGen focuses on the *shape* and *complementarity* of the interaction surface rather than the precise position of

every atom. This mirrors how expert medicinal chemists often reason about the “key interactions” (e.g., a specific salt bridge or hydrophobic pocket) rather than the entire protein volume.

6.2. Efficiency and High-Throughput Readiness

The reduction of memory scaling from $O(L^2)$ to $O(K^2)$ enables two major use cases. First, it allows for the generation of ligands for large, multi-subunit protein complexes (e.g., ribosome-bound inhibitors) that are currently beyond the reach of dense structural generators. Second, it enables **generative virtual screening**, where the model can be conditioned on thousands of different pocket conformations (from MD simulations) in a fraction of the time required for physics-based docking.

6.3. Synthesizability and Reaction-Awareness

While SiDGen achieves 100% validity and high diversity, the generation of “drug-like” molecules also requires consideration of synthesizability. Unlike 3D generators that may produce strained geometries, SiDGen’s SMILES-space transformer denoiser (Chemformer-style architecture) encourages outputs that remain consistent with the known chemical manifold of druglike SMILES. Future iterations will investigate the integration of reaction-aware tokens, as proposed in **RxnFlow** (Seo et al., 2025), to further improve the down-stream utility of the generated hits.

6.4. Limitations and Future Work

The primary limitation of SiDGen is the absence of an explicit 3D pose for the generated ligand. Although the Vina Dock scores are high, these require an external docking step at inference. We are currently developing a “joint-diffusion” variant in which the TIB conditions both the SMILES generation and a coarse-grained 3D pose prediction. This would allow for end-to-end “pose-aware” generation without sacrificing the efficiency of the topological bottleneck.

7. Conclusion

We have presented **SiDGen**, a hierarchical structural diffusion model that resolves the scaling-fidelity dilemma in SBDD. By introducing the Topological Information Bottleneck via learned soft assignment pooling (DiffPool-inspired), we achieve a significant reduction in pairwise-tensor complexity while maintaining state-of-the-art binding affinities and virtual screening performance. SiDGen demonstrates that efficient, pocket-aware molecular generation is achievable through structured topological compression, providing a scalable and expressive framework for the next generation of AI-driven drug discovery.

Impact Statement

This paper is aimed to facilitate in-silico rational drug design. Potential society consequences include mal-intended usage of toxic compound discovery, which needs support from professional wet labs and thus expensive to reach. Therefore we do not possess a negative vision that this might lead to serious ethical consequences, though we are aware of such a possibility.

References

Bickerton, G. R., Paolini, G. V., Besnard, J., Muresan, S., and Hopkins, A. L. Quantifying the chemical beauty of drugs. *Nature Chemistry*, 4(2):90–98, 2012. doi: 10.1038/nchem.1243. URL <https://www.nature.com/articles/nchem.1243>.

Chang, J. and Ye, J. C. LDMol: A text-to-molecule diffusion model with structurally informative latent space surpasses AR models. In *Forty-second International Conference on Machine Learning*, 2025. URL <https://openreview.net/forum?id=16mkb1LBVP>.

Eberhardt, J., Santos-Martins, D., Tillack, A. F., and Forli, S. Autodock vina 1.2.0: New docking methods, expanded force field, and python bindings. *Journal of Chemical Information and Modeling*, 61(8):3891–3898, 2021. doi: 10.1021/acs.jcim.1c00203. URL <https://doi.org/10.1021/acs.jcim.1c00203>. PMID: 34278794.

Elfwing, S., Uchibe, E., and Doya, K. Sigmoid-weighted linear units for neural network function approximation in reinforcement learning, 2017. URL <https://arxiv.org/abs/1702.03118>.

Ertl, P. and Schuffenhauer, A. Estimation of synthetic accessibility score of drug-like molecules based on molecular complexity and fragment contributions. *Journal of cheminformatics*, 1:8, 06 2009. doi: 10.1186/1758-2946-1-8.

Francoeur, P. G., Masuda, T., Sunseri, J., Jia, A., Iovanisci, R. B., Snyder, I., and Koes, D. R. Three-dimensional convolutional neural networks and a cross-docked data set for structure-based drug design. *Journal of Chemical Information and Modeling*, 60(9):4200–4215, 2020. doi: 10.1021/acs.jcim.0c00411. URL <https://doi.org/10.1021/acs.jcim.0c00411>. PMID: 32865404.

Friesner, R. A., Murphy, R. B., Repasky, M. P., Frye, L. L., Greenwood, J. R., Halgren, T. A., Sanschagrin, P. C., and Mainz, D. T. Extra precision glide: Docking and scoring incorporating a model of hydrophobic enclosure for protein-ligand complexes. *Journal of Medicinal Chemistry*, 49(21):6177–6196, 2006. doi: 10.1021/jm051256o. URL <https://doi.org/10.1021/jm051256o>. PMID: 17034125.

Gao, B., Huang, Y., Liu, Y., Xie, W., Ma, W.-Y., Zhang, Y.-Q., and Lan, Y. Pushing the boundaries of structure-based drug design through collaboration with large language models. 2025. URL <https://arxiv.org/abs/2503.01376>.

Gómez-Bombarelli, R., Duvenaud, D., Hernández-Lobato, J. M., Aguilera-Iparraguirre, J., Hirzel, T. D., Adams, R. P., and Aspuru-Guzik, A. Automatic chemical design using a data-driven continuous representation of molecules. *CoRR*, abs/1610.02415, 2016. URL <http://arxiv.org/abs/1610.02415>.

Guan, J., Qian, W. W., Peng, X., Su, Y., Peng, J., and Ma, J. 3d equivariant diffusion for target-aware molecule generation and affinity prediction. 2023a. URL <https://arxiv.org/abs/2303.03543>.

Guan, J., Zhou, X., Yang, Y., Bao, Y., Peng, J., Ma, J., Liu, Q., Wang, L., and Gu, Q. Decomppdiff: diffusion models with decomposed priors for structure-based drug design. 2023b.

Guharoy, M. and Chakrabarti, P. Conserved residue clusters at protein–protein interfaces and their use in binding site identification. *BMC Bioinformatics*, 11:286, May 2010. doi: 10.1186/1471-2105-11-286. URL <https://doi.org/10.1186/1471-2105-11-286>.

Hoogeboom, E., Satorras, V. G., Vignac, C., and Welling, M. Equivariant diffusion for molecule generation in 3d. 2022. URL <https://arxiv.org/abs/2203.17003>.

Irwin, R., Dimitriadis, S., He, J., and Bjerrum, E. J. Chemformer: a pre-trained transformer for computational chemistry. *Machine Learning: Science and Technology*, 3, 2021. URL <https://api.semanticscholar.org/CorpusID:237747003>.

Jumper, J. M., Evans, R., Pritzel, A., Green, T., Figurnov, M., Ronneberger, O., Tunyasuvunakool, K., Bates, R., Žídek, A., Potapenko, A., Bridgland, A., Meyer, C., Kohl, S. A. A., Ballard, A., Cowie, A., Romera-Paredes, B., Nikolov, S., Jain, R., Adler, J., Back, T., Petersen, S., Reiman, D., Clancy, E., Zielinski, M., Steinegger, M., Pacholska, M., Berghammer, T., Bodenstein, S., Silver, D., Vinyals, O., Senior, A. W., Kavukcuoglu, K., Kohli, P., and Hassabis, D. Highly accurate protein structure prediction with alphafold. *Nature*, 596:583 – 589, 2021. URL <https://api.semanticscholar.org/CorpusID:235959867>.

Lin, Z., Akin, H., Rao, R., Hie, B., Zhu, Z., Lu, W., Smetanin, N., Verkuil, R., Kabeli, O., Shmueli, Y., dos Santos Costa, A., Fazel-Zarandi, M., Sercu, T., Candido, S., and Rives, A. Evolutionary-scale prediction of atomic level protein structure with a language model.

bioRxiv, 2022. doi: 10.1101/2022.07.20.500902. URL <https://www.biorxiv.org/content/early/2022/10/31/2022.07.20.500902>.

McNutt, A., Francoeur, P., Aggarwal, R., Masuda, T., Meli, R., Ragoza, M., Sunseri, J., and Koes, D. Gnina 1.0: Molecular docking with deep learning. *ChemRxiv*, 2021. doi: 10.26434/chemrxiv.13578140.v1.

Mistryukova, L., Manuilov, V., Avchaciov, K., and Fedichev, P. O. Protobind-diff: A structure-free diffusion language model for protein sequence-conditioned ligand design. *bioRxiv*, 2025. doi: 10.1101/2025.06.16.659955. URL <https://www.biorxiv.org/content/early/2025/06/20/2025.06.16.659955>.

Mysinger, M. M., Carchia, M., Irwin, J. J., and Shoichet, B. K. Directory of useful decoys, enhanced (dud-e): Better ligands and decoys for better benchmarking. *Journal of Medicinal Chemistry*, 55(14):6582–6594, 2012. doi: 10.1021/jm300687e. URL <https://doi.org/10.1021/jm300687e>. PMID: 22716043.

Peng, X., Luo, S., Guan, J., Xie, Q., Peng, J., and Ma, J. Pocket2mol: Efficient molecular sampling based on 3d protein pockets. 2025. URL <https://arxiv.org/abs/2205.07249>.

Polykovskiy, D., Zhebrak, A., Sanchez-Lengeling, B., Golovanov, S., Tatanov, O., Belyaev, S., Kurbanov, R., Artamonov, A., Aladinskiy, V., Veselov, M., Kadurin, A., Johansson, S., Chen, H., Nikolenko, S., Aspuru-Guzik, A., and Zhavoronkov, A. Molecular sets (moses): A benchmarking platform for molecular generation models. *Frontiers in Pharmacology*, Volume 11 - 2020, 2020. ISSN 1663-9812. doi: 10.3389/fphar.2020.565644. URL <https://www.frontiersin.org/journals/pharmacology/articles/10.3389/fphar.2020.565644>.

Preuer, K., Renz, P., Unterthiner, T., Hochreiter, S., and Klambauer, G. Fréchet chemnet distance: A metric for generative models for molecules in drug discovery. 2018. URL <https://arxiv.org/abs/1803.09518>.

Qiu, K., Song, Y., Fan, Z., Liu, P., Zhang, Z., Zheng, M., Zhou, H., and Ma, W.-Y. Piloting structure-based drug design via modality-specific optimal schedule. *ICML* 2025, 2025.

Qu, Y., Qiu, K., Song, Y., Gong, J., Han, J., Zheng, M., Zhou, H., and Ma, W.-Y. Molcraft: Structure-based drug design in continuous parameter space. *ICML* 2024, 2024.

Ross, J., Belgodere, B., Chenthamarakshan, V., Padhi, I., Mroueh, Y., and Das, P. Do large scale molecular language representations capture important structural information? *CoRR*, abs/2106.09553, 2021. URL <https://arxiv.org/abs/2106.09553>.

Seo, S., Kim, M., Shen, T., Ester, M., Park, J., Ahn, S., and Kim, W. Y. Generative flows on synthetic pathway for drug design. In *The Thirteenth International Conference on Learning Representations*, 2025. URL <https://openreview.net/forum?id=pB1XSj2y4X>.

Su, J., Lu, Y., Pan, S., Wen, B., and Liu, Y. Roformer: Enhanced transformer with rotary position embedding. *CoRR*, abs/2104.09864, 2021. URL <https://arxiv.org/abs/2104.09864>.

Vignac, C., Krawczuk, I., Siraudin, A., Wang, B., Cevher, V., and Frossard, P. Digress: Discrete denoising diffusion for graph generation. 2023. URL <https://arxiv.org/abs/2209.14734>.

Ying, R., You, J., Morris, C., Ren, X., Hamilton, W. L., and Leskovec, J. Hierarchical graph representation learning with differentiable pooling. volume abs/1806.08804, 2018. URL <http://arxiv.org/abs/1806.08804>.

Zhao, W., Hevener, K. E., White, S. W., Lee, R. E., and Boyett, J. M. A statistical framework to evaluate virtual screening. *BMC Bioinformatics*, 10(1):225, 2009. doi: 10.1186/1471-2105-10-225. URL <https://doi.org/10.1186/1471-2105-10-225>.

A. Detailed Experimental Configuration

A.1. Data Preprocessing

- **SMILES Canonicalization:** SMILES are tokenized with a Chemformer-style SMILES tokenizer (the JSON tokenizer used in the repo); on-the-fly SMILES randomization is enabled.
- **Sequence Processing:** We use precomputed ESM-2 embeddings loaded; sequences are padded per-batch using length-aware batching.
- **Metadata Files:** The diffusion dataset index (data.csv) contains 1,154,055 entries, and categorical mappings include 793,429 entries; the tokenizer vocabulary size is 54 tokens.
- **Data Splitting:** Random train/validation/test split of 80/10/10 (923,244 / 115,406 / 115,405 samples; total 1,154,055) with seed 188.

A.2. Model Architecture Details

- **Transformer Configuration:** 4 decoder layers, hidden dimension $H = 1280$, 8 attention heads ($d_{\text{head}} = 160$), FFN intermediate dimension $3H = 3840$
- **Pooling/Folding Parameters:** Stride $s = 4$, pair dimension $C_{\text{pair}} = 64$, folding heads 8, folding head dim 16, transition factor 3.
- **Vocabulary:** SMILES tokenizer with 54 tokens including standard SMILES characters (C, N, O, etc.), brackets, ring numbers, special tokens ([MASK], [PAD], [BOS], [EOS])
- **Maximum Lengths:** Protein $L_{\text{max}} = 1024$ (evaluation), SMILES $L_{\text{SMILES}} = 1700$ (training default)
- **Position Encodings:** RoPE (base 10000) applied in ligand self-attention; cross-attention uses standard dot-product attention.
- **Layer Normalization:** Decoder uses post-norm residual blocks (Add \rightarrow LayerNorm); folding modules use LayerNorm without affine parameters.

A.3. Training Details

- **Optimizer:** AdamW with $\beta_1 = 0.9$, $\beta_2 = 0.999$, $\epsilon = 10^{-8}$, weight decay 0.01
- **Learning Rate Schedule:** Constant learning rate 10^{-4} (AdamW) for all training steps.
- **Batch Configuration:** Max per-device batch size 16, batch volume 8,000,000, gradient accumulation steps 2
- **Gradient Clipping:** Max norm 1.0 applied to global gradient norm
- **Curriculum Learning:** $T_{\text{curriculum}} = 2$ epochs, linearly increasing α_{epoch} from 0.1 to 1.0
- **Validity Penalty:** $\lambda_{\text{valid}} = 0.1$, computed on 32 mini-batch samples every 100 steps using RDKit SMILES validation
- **Training Duration:** 10 epochs on 1,154,055 samples (steps depend on effective batch size)
- **Precision:** bf16 mixed precision (float type `bfloat16`)
- **Hardware:** A100-class GPUs; peak per-GPU VRAM ≈ 60 GB (including batch + backprop)
- **Checkpointing:** Model checkpoints saved every `checkpoint_every=10000` optimizer steps; best model selected based on validation SMILES validity.

A.4. Inference Configuration

- **Sampling Steps:** $T = 100$ diffusion steps with log-linear noise schedule
- **Temperature:** 1.0 (no temperature scaling for sampling)
- **Top-k/Top-p:** Nucleus sampling with $p = 0.9$; no top-k
- **Noise Parameters:** $\eta = 0.1$, noise removal enabled
- **Guidance:** Classifier-free guidance disabled ($w = 0$, `cfg_every_k=0`)
- **Generation Count:** 100 molecules per target protein for all evaluations
- **Post-processing:** Generated SMILES are canonicalized and validated with RDKit.

A.5. Evaluation Protocol Details

- **Docking Setup:** We use a fixed docking engine (AutoDock Vina) with a single standardized protocol across baselines: identical search box sizes, exhaustiveness, and number of poses retained. We report Vina Dock (kcal/mol) on the top-ranked pose.
- **Success Rate:** A generated pose is counted as a success if it achieves Vina Dock \leq a target-specific threshold and is within 2.0 Å RMSD of the redocked conformation (when a reference ligand is available).
- **Synthesizability:** We report SA score (Ertl & Schuffenhauer, 2009) and QED (Bickerton et al., 2012) for all generated molecules, matching evaluation protocols in recent SBDD benchmarks.

A.6. Molecular Property Distributions

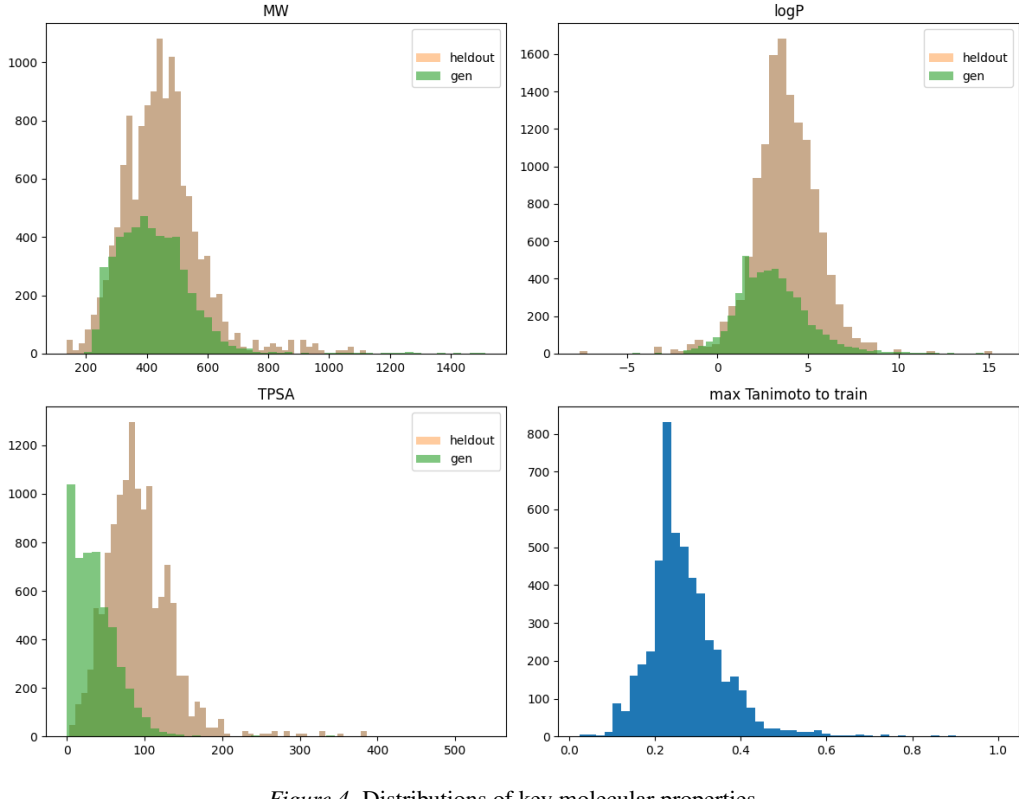


Figure 4. Distributions of key molecular properties

This figure compares generated (gen) vs holdout distributions for molecular weight (MW), logP, TPSA, and maximum Tanimoto similarity to the training set. The shown run reports mean MW 421.57, mean logP 3.07, mean TPSA 37.89, mean max-Tanimoto 0.27, and SA score 0.49.

B. Complete Ablation Studies

B.1. Bottleneck Coarse Dimension

Table 5 shows comprehensive performance vs. coarse dimension K for fixed protein length $L = 592$ during inference with $batch_size = 1$.

Table 5. Effect of bottleneck coarse dimension K on CrossDocked2020 performance (full results)

Stride s	VRAM (GiB)	Vina Dock	QED	Diversity
16	0.17	-8.91	0.52	0.89
8	0.67	-9.28	0.54	0.88
4	2.67	-9.81	0.58	0.90
2	10.70	-9.83	0.58	0.89
1	42.78	-9.87	0.59	0.91

$K = 128$ ($s = 4$) provides the best performance-efficiency trade-off. Pair-tensor VRAM drops from 42.78 GiB ($s = 1$) to 2.67 GiB ($s = 4$) at $L = 592$, while preserving near-optimal binding. Very coarse pooling ($K = 37$, stride 16) shows 0.96 kcal/mol degradation, confirming the need for sufficient spatial resolution.

B.2. Pooling Ablation: Learned Pooling vs. Coarse Striding

We compare learned soft-assignment pooling against a coarse strided pooling baseline (index-select downsampling) at the same stride s .

Table 6. Pooling ablation at fixed stride $s = 4$ (CrossDocked2020).

Pooling	Vina Dock	QED	SA
Coarse Striding	-9.74	0.55	0.47
Learned Pooling	-9.81	0.58	0.49

C. Cross-Family Performance Analysis

Table 7 shows detailed performance breakdown by PFAM family on CrossDocked2020 test set.

Table 7. Performance by protein family (top 5 families by sample count in test set)

PFAM Family	Count	Vina Dock	QED
Kinase (PF00069)	1247	-9.89	0.56
GPCR (PF00001)	892	-9.21	0.54
Protease (PF00082)	634	-10.11	0.57
Nuclear Receptor (PF00104)	421	-9.43	0.55
Ion Channel (PF00520)	318	-8.97	0.52
Overall	3512	-9.81	0.58

Performance is consistent across major drug target families. Proteases show the strongest binding affinity (-10.11 kcal/mol), likely due to well-defined active sites. GPCRs and ion channels show slightly lower scores, potentially due to more flexible binding pockets. The 100% validity across all families demonstrates robustness.

D. Architectural Details

D.1. Latent-variable View of the Bottleneck

Conceptually, protein-conditioned generation can be written as a latent-variable model

$$p(x | \mathcal{P}) = \int_{\mathcal{Z}} p(x | z) p(z | \mathcal{P}) dz. \quad (38)$$

In **SiDGen**'s implementation, the bottleneck is computed via pooling, i.e., $z = z(\mathcal{P})$. This corresponds to a degenerate posterior $p(z | \mathcal{P}) = \delta(z - z(\mathcal{P}))$, yielding

$$p(x | \mathcal{P}) = p(x | z(\mathcal{P})), \quad (39)$$

which is the view used throughout the paper's main sections and matches the training/inference codepath.

D.2. Decoder Architecture

The denoiser is a Transformer decoder operating on masked SMILES token embeddings, with cross-attention into a conditioning context built from a timestep token and bottleneck tokens z and additional protein tokens. The implementation uses post-norm residual blocks (Add \rightarrow LayerNorm).

Timestep token. We embed timesteps $t \in \mathbb{R}^B$ using sinusoidal features $\text{PE}(t)$ followed by a 2-layer MLP:

$$\tau(t) = \text{SiLU}(W_2 \text{SiLU}(W_1 \text{PE}(t))) \in \mathbb{R}^H. \quad (40)$$

Sequences. Let $\mathbf{X}_{\text{lig}} \in \mathbb{R}^{B \times L \times H}$ be ligand token embeddings and $\mathbf{Z} \in \mathbb{R}^{B \times K \times H}$ be the bottleneck tokens. The cross-attention context is

$$\mathbf{C} = [\tau(t); \mathbf{Z} (\mathbf{X}_{\text{prot}})]. \quad (41)$$

In the implemented model, $\tau(t)$ participates in cross-attention as part of \mathbf{C} and is not appended to the ligand sequence for self-attention.

RoPE. Rotary position embeddings (RoPE) are applied to ligand self-attention queries/keys with base frequency 10000; cross-attention uses standard dot-product attention.

One decoder block. For layer ℓ , with post-norm residual connections:

$$\mathbf{X}'_{\ell} = \text{LN}(\mathbf{X}_{\ell-1} + \text{MHA}(\mathbf{X}_{\ell-1})), \quad (42)$$

$$\mathbf{X}''_{\ell} = \text{LN}(\mathbf{X}'_{\ell} + \text{CrossMHA}(\mathbf{X}'_{\ell}, \mathbf{C})), \quad (43)$$

$$\mathbf{X}_{\ell} = \text{LN}(\mathbf{X}''_{\ell} + \text{FFN}(\mathbf{X}''_{\ell})), \quad (44)$$

where MHA is multi-head self-attention over the ligand sequence (with RoPE), CrossMHA is multi-head cross-attention into \mathbf{C} , and $\text{FFN}(x) = W_2 \phi(W_1 x + b_1) + b_2$ with nonlinearity ϕ .

The final hidden states are projected to vocabulary logits to predict token distributions required by the masked diffusion objective.

D.3. Training Objective

We optimize a masked diffusion objective on SMILES tokens with noise level $\sigma(t)$:

$$\mathcal{L}_{\text{MDLM}} = -\mathbb{E}_{x_0, t} \log p_{\theta}(x_0 | x_t, \mathcal{P}) \cdot \frac{d\sigma/dt}{\exp(\sigma) - 1}, \quad (45)$$

$$x_t \sim q(x_t | x_0, \sigma(t)), \quad (46)$$

where x_t is produced by masking tokens with probability $1 - \exp(-\sigma(t))$ and \mathcal{P} is the conditioning context.

D.4. Forward Process (Discrete Masking)

Let $m(t) = 1 - \exp(-\sigma(t))$ be the mask probability. For each token $x_0^{(i)}$, we sample

$$q(x_t^{(i)} = [\text{MASK}] \mid x_0^{(i)}) = m(t), \quad (47)$$

$$q(x_t^{(i)} = x_0^{(i)} \mid x_0^{(i)}) = 1 - m(t), \quad (48)$$

and apply this independently over positions. The resulting x_t is embedded and passed to the decoder.

D.5. SUBS Parameterization

We use the substitution (SUBS) parameterization: logits for the mask token are set to $-\infty$ and unmasked positions are constrained to remain unchanged,

$$\log p_\theta(x_{t-1} \mid x_t) \leftarrow \log p_\theta(x_{t-1} \mid x_t) - \log Z, \quad (49)$$

$$\log p_\theta(x_{t-1} = x_t \mid x_t \neq [\text{MASK}]) = 0. \quad (50)$$

D.6. Training Algorithm (High Level)

Given batch (\mathcal{P}, x_0) , we sample $t \sim \mathcal{U}[0, 1]$, mask x_0 to obtain x_t , run the decoder with conditioning \mathcal{P} , and minimize $\mathcal{L}_{\text{MDLM}}$ with AdamW. Mixed precision (bf16) and gradient accumulation are used for efficiency.

Algorithm 1 Training (Masked Diffusion)

- 1: Sample $t \sim \mathcal{U}(0, 1)$ and compute $\sigma(t)$
- 2: Mask tokens with probability $m(t) = 1 - \exp(-\sigma(t))$ to obtain x_t
- 3: Forward: $(\hat{x}_0, \cdot) = f_\theta(\mathcal{P}, x_t, \sigma(t))$
- 4: Compute $\mathcal{L}_{\text{MDLM}}$ and backpropagate with AdamW (bf16 + grad accumulation)

D.7. Sampling Algorithm

At inference, we iterate t from 1 to ϵ in T steps, denoise x_t with the decoder, and sample the next tokens using nucleus sampling ($p = 0.9$). A final noise-removal pass produces x_0 .

Algorithm 2 Sampling (ReMDM-cap + SUBS)

- 1: Initialize $x_T \leftarrow [\text{MASK}]$ tokens
- 2: Set a timestep grid $t_0 = 1 > t_1 > \dots > t_T = \epsilon$ with step size Δt
- 3: **for** $i = 1$ to T **do**
- 4: Compute $\sigma_i = \sigma(t_i)$ and mask probability $m_i = 1 - \exp(-\sigma_i)$
- 5: Predict normalized log-probabilities $\log p_\theta(x_0 \mid x_{t_i})$ and apply SUBS parameterization (mask token suppressed; unmasked tokens fixed)
- 6: Convert to $p_\theta(x_0 \mid x_{t_i})$ (apply temperature schedule and nucleus top- p)
- 7: Let $\alpha_i = 1 - m_i$ and $\alpha_{i-1} = 1 - m_{i-1}$ and set the capped noise $\tilde{\eta} = \min\left(\eta, \frac{1-\alpha_{i-1}}{\alpha_i}\right)$
- 8: Form the categorical proposal $q(x_{t_{i-1}} \mid x_{t_i})$ by mixing $p_\theta(x_0 \mid x_{t_i})$ with the mask token at rate $\tilde{\eta}$ (ReMDM-cap)
- 9: Sample $x_{t_{i-1}} \sim q(\cdot \mid x_{t_i})$
- 10: **end for**
- 11: Noise-removal step at $t = \epsilon$

E. Triangle Operators

We provide detailed formulations of the triangle attention and multiplication operators applied to coarse pair features $\mathbf{p}_c \in \mathbb{R}^{B \times K \times K \times C}$. Each operator follows the same pattern: (i) layer-normalize the pair features, (ii) project into head space, (iii) apply attention or bilinear interaction, (iv) gate and project back to C .

E.1. Triangle Attention

Starting Node Update:

$$\tilde{\mathbf{p}} = \text{LN}(\mathbf{p}_c), \quad (51)$$

$$\mathbf{q}_i = W_Q \tilde{\mathbf{p}}_{i,:}, \quad \mathbf{k}_i = W_K \tilde{\mathbf{p}}_{i,:}, \quad \mathbf{v}_i = W_V \tilde{\mathbf{p}}_{i,:}, \quad (52)$$

$$\alpha_{i,j,k} = \text{softmax}_k \left(\frac{\langle \mathbf{q}_{i,j}, \mathbf{k}_{i,k} \rangle}{\sqrt{d_h}} + b_{i,j,k} \right), \quad (53)$$

$$\mathbf{o}_{i,j} = \sum_k \alpha_{i,j,k} \mathbf{v}_{i,k}, \quad (54)$$

$$\mathbf{p}_c[b, i, j] \leftarrow W_O(\sigma(W_G \tilde{\mathbf{p}}_{i,j}) \odot \mathbf{o}_{i,j}) \quad (55)$$

For fixed batch b and row i , each edge (i, j) attends to all edges (i, k) sharing the starting node i . The bias $b_{i,j,k}$ is derived from pair features and a mask.

Ending Node Update:

$$\mathbf{p}_c[b, i, j] \leftarrow \text{TriAttn}_{\text{end}}(\mathbf{p}_c[b, \cdot, j]) \quad (56)$$

For fixed batch b and column j , each edge (i, j) attends to all edges (k, j) sharing the ending node j .

E.2. Triangle Multiplication

Outgoing Edges:

$$\tilde{\mathbf{p}} = \text{LN}(\mathbf{p}_c), \quad (57)$$

$$\mathbf{a}_{i,k} = W_A \tilde{\mathbf{p}}_{i,k}, \quad \mathbf{b}_{j,k} = W_B \tilde{\mathbf{p}}_{j,k}, \quad (58)$$

$$\mathbf{p}_c[b, i, j] \leftarrow \sigma(W_G \tilde{\mathbf{p}}_{i,j}) \odot W_O \left(\sum_{k=1}^K \mathbf{a}_{i,k} \odot \mathbf{b}_{j,k} \right) \quad (59)$$

where g and h are linear projections. This aggregates information over paths $i \rightarrow k \leftarrow j$.

Incoming Edges:

$$\mathbf{p}_c[b, i, j] \leftarrow \sigma(W_G \tilde{\mathbf{p}}_{i,j}) \odot W_O \left(\sum_{k=1}^K \mathbf{a}_{k,i} \odot \mathbf{b}_{k,j} \right) \quad (60)$$

This aggregates information over paths $i \leftarrow k \rightarrow j$.

These operations enforce geometric consistency in the learned pairwise features by leveraging triangle inequality constraints, similar to AlphaFold's protein structure prediction.

E.3. Transition Factor Usage

The `transition_factor` controls the width expansion in the single and pair transition MLPs :

$$\text{SingleFC} : \mathbb{R}^{C_{\text{single}}} \rightarrow \mathbb{R}^{r C_{\text{single}}} \rightarrow \mathbb{R}^{C_{\text{single}}}, \quad (61)$$

$$\text{PairFC} : \mathbb{R}^{C_{\text{pair}}} \rightarrow \mathbb{R}^{r C_{\text{pair}}} \rightarrow \mathbb{R}^{C_{\text{pair}}}, \quad (62)$$

E.4. Operator Masking and Stability

We apply a pairwise mask $M \in \{0, 1\}^{K \times K}$ derived from sequence padding. For attention, invalid keys are masked by adding $-\infty$ to logits. For multiplication, invalid entries are zeroed before aggregation. Gating terms $\sigma(W_G \cdot)$ stabilize training by limiting updates to confident edges.

E.5. FoldingBlock Algorithm

We follow the implementation order in FoldingBlock:

Algorithm 3 FoldingBlock (coarse grid)

```
1:  $M \leftarrow$  mask;  $s, p$  are single/pair features
2:  $s \leftarrow s + \text{SingleAttn}(s, M, \text{attn\_bias}(p))$ 
3:  $s \leftarrow s + \text{SingleFC}(s; r = \text{transition\_factor})$ 
4:  $p \leftarrow p + \text{OuterLinear}(s)$ 
5:  $p \leftarrow p + \text{TriMult}_{\text{out}}(p, M)$ 
6:  $p \leftarrow p + \text{TriMult}_{\text{in}}(p, M)$ 
7:  $p \leftarrow p + \text{TriAttn}_{\text{start}}(p, M)$ 
8:  $p \leftarrow p + \text{TriAttn}_{\text{end}}(p, M)$ 
9:  $p \leftarrow p + \text{PairFC}(p; r = \text{transition\_factor})$ 
10: return  $s, p$ 
```
